ACS APPLIED MATERIALS & INTERFACES

www.acsami.org

Research Article

Does Bacterial Elasticity Affect Adhesion to Polymer Fibers?

Laura Tamayo,* Francisco Melo,* Leonardo Caballero, Eugenio Hamm, M. Díaz, M. S. Leal, N. Guiliani, and M. D. Urzúa

Cite This: *ACS Appl. Mater. Interfaces* 2020, 12, 14507−14517

Read Online

ACCESS | Metrics & More | Article Recommendations | Supporting Information

ABSTRACT: The factors governing bacterial adhesion to substrates with different topographies are still not fully identified. The present work seeks to elucidate for the first time and with quantitative data the roles of bacterial elasticity and shape and substrate topography in bacterial adhesion. With this aim, populations of three bacterial species, *P. aeruginosa* DSM 22644, *B. subtilis* DSM 10, and *S. aureus* DSM 20231 adhered on flat substrates covered with electrospun polycaprolactone fibers of different diameters ranging from 0.4 to 5.5 μm are counted. Populations of bacterial cells are classified according to the preferred binding sites of the bacteria to the substrate. The colloidal probe technique was used to assess the stiffness of the bacteria and bacteria−polymer surface adhesion energy. A theoretical model is developed to interpret the observed populations in terms of a balance between stiffness and adhesion energy of the bacteria. The model, which also incorporates the radius of the fiber and the size and shape of the bacteria, predicts increased adhesion for a low level of stiffness and for a larger number of available bacteria−fiber contact points. Te adhesive propensity of bacteria depends in a nontrivial way on the radius of the fibers due to the random arrangement of fibers.

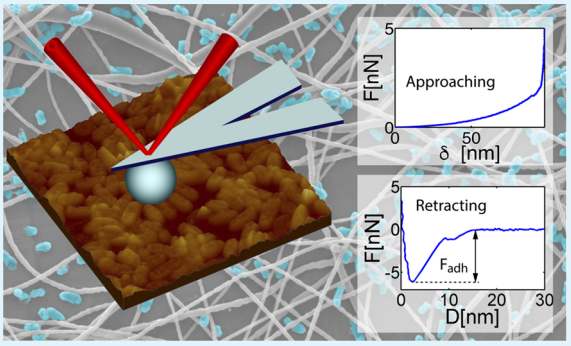

KEYWORDS: *bacteria, adhesion, fibers, elasticity, polymer surfaces*

INTRODUCTION

Much of the materials used today to manufacture medical devices like wound dressings, implant coatings, cell regeneration supports, and vascular stents are made of polymeric fibers.[1−3] The polymer fiber collection at the micro- and nanoscales has given rise to polymeric meshes with highly exposed surfaces and high degrees of porosity and permeability, which allow the absorption of fluids and promote respiration and cell proliferation.[4−6] These characteristics make polymer fiber meshes ideal for manufacturing medical devices, although the susceptibility of these materials to bacterial adherence and proliferation and consequent infection represents a serious obstacle to their use.[7] *S. aureus* is one the main pathogens that cause infections in medical devices due to its ability to form biofilm.[8] Heart valves and artificial joints are especially vulnerable to bacterial colonization by this bacterium.[9] *P. aeruginosa* has been identified as one of the most important pathogens of nosocomial infections due to its ability to form biofilms on most medical devices, greater resistance/tolerance to antibiotics, opportunistic pathogenicity, and persistence in hospital environments.[10] Diseases like ventilator-associated pneumonia and urinary tract infections are caused by colonization of pathogens such as *P. aeruginosa*.[11,12]

Understanding the behavior of bacterial adhesion to abiotic surfaces is crucial to develop strategies to control bacterial colonization. However, to date, the study of the bacterial adhesion on surfaces made from fibers has been poorly explored.[13,14] Bacterial adhesion to any surface can be explained based on the interactions between the surface of the bacteria and the abiotic surface of a substrate. These interactions can be the result of additive factors from attractive interactions such as van der Waals interactions and repulsive interactions such as the superposition of the electrical double layer between the surface of the bacteria and the substrate, as explained by the Derjaguin−Landau−Verwey−Overbeek (DLVO) theory.[15] According to this theory, there are two temporal phases in adhesion: the reversible phase and the irreversible phase. The first considers the bacterial cell as an almost inert colloidal particle that binds to the surface, according to physicochemical predictions, while the second considers the biological activity of the bacteria based on the generation of biopolymers that promote adhesion. The thermodynamic theory also explains bacterial adhesion through attractive and repulsive interactions, but they are expressed in terms of adhesion-free energy, with quantitative values of the free energy from the surface of the bacteria and substrate.

Received: November 19, 2019
Accepted: March 2, 2020
Published: March 2, 2020

Table 1. Parameters for Electrospun Fibers and the Influence of the Proportion of Solvents, Conductivity, and Surface Tension on Fiber Diameter

sample	PCL solution (w/v%)	ratio solvent DCM/DMF	flow rate (mL/min)	voltage applied (kV)	conductivity (mS/cm)	surface tension (mN/m)	fiber diameter (μm)
F1	15	0/100	1.0	14.5	0.42	37.60 ± 0.29	0.4 ± 0.2
F2		50/50	1.4	15.0	0.23	39.10 ± 0.15	0.8 ± 0.4
F3		85/15	2.0	18.0	0.05	46.20 ± 0.06	1.8 ± 0.7
F4		75/25	2.5	18.0	0.06	45.10 ± 0.06	3.6 ± 0.3

Unlike the DLVO theory, the thermodynamic approach considers that adhesion is always reversible. A third theory, the extended DLVO theory additionally considers acid−base interactions, which correspond to attractive hydrophobic interactions and repulsive hydration effects, which are 10−100 times as strong as van der Waals interactions.[16]

Although several theories have been developed to explain the mechanisms of bacterial adhesion, adhesion is a complex process, controlled by many factors, such as bacterial membrane/wall composition, substrate composition, environmental factors like pH and ionic strength, and other physical and topographic parameters. In particular, it has been observed that the topographic (roughness) and geometric characteristics of substrates directly affect the adhesive behavior of bacteria, an aspect considered by the extended DLVO model, while the classical DLVO theory and thermodynamic approaches consider the substrate as a perfectly smooth surface.[17] In fact, topography at the micro- and nanoscales has been identified as a determining factor in bacterial adhesion. Studies have established several premises that predict increased or decreased bacterial adhesion to particular substrates. However, the results of many of these studies are controversial.[18,19] Several works have studied the effect of the topography of substrates prepared by lithography, which produces regular patterns at the micro- and nanoscales, such as grooves, pits, pillars, and honeycombs, among others.[20−22] Surfaces with microscale patterns have increased bacterial adhesion, which is attributed to more contact surface and less shear force under a moving fluid.[23] These studies have shown that bacteria tend to bind preferentially to patterns in the micrometer range rather than to smooth surfaces. The general premise is that bacteria preferentially adhere to patterns with dimensions similar to those of the bacteria.[24] However, there have been contradictory findings at the nanoscale. For example, *Escherichia coli* and *Pseudomonas aeruginosa* are apparently less adherent when the surface pattern is smaller than the bacterial size,[25,26] but some studies have shown that the surface patterns at the nanoscale do not affect the adhesion of these same two bacteria.[27,28] Although the studies of bacterial adherence to regular patterns at the micro- and nanoscales have provided important information on the factors governing bacterial adherence to these structures, the problem of bacterial colonization on medical devices involves irregular surfaces so that adhesion studies on surfaces made of fibers are more appropriate for developing strategies to control bacterial proliferation in this context. While there have been numerous studies of eukaryotic cell adhesion to fibers (fibroblasts, osteoblasts, endothelial cells) and the effect of the topographic characteristics of meshes on cell adhesion, proliferation, and differentiation,[29,30] there have been a few studies on the factors that promote or minimize bacterial adhesion to fibers.[31]

Some works have studied bacterial adhesion to irregular surfaces, particularly involving rough surfaces. A study of the effect of the roughness of glass surfaces modified with chemical etching on the adhesion of *Pseudoalteromonas issachecnkonii* KMM 3549T demonstrated that roughness at the nanoscale increases bacterial adhesion.[32] This result casts doubt on the premise that bacteria adhere mainly to surfaces with topographic characteristics of similar dimensions to that of the bacteria. Other studies have pointed to an optimal level of roughness to minimize adhesion. Specifically, the topography of titanium surfaces has been evaluated in terms of average arithmetic roughness (R_a). It was found that surfaces with R_a in the range of 0.43−1.25 μm have a significant impact on the adhesion of *Staphylococcus epidermidis*.[33] Bacteria adhere less to stainless steel surfaces with an average roughness of 0.16 μm than to either smoother or rougher stainless steel surfaces.[34] Most works have attributed dissimilarities in bacterial adhesion to differences in the cell shape (spherical, rod-shaped) or the composition of the cell envelope (Gram-positive or Gram-negative).[27,28]

Studies on the effect of substrate stiffness on bacterial adhesion have found that adhesion correlates positively with the elastic modulus of polyelectrolyte substrates, reducing the significance of other factors like roughness, interaction energy, and charge density.[35] In contrast, other works have determined that soft substrates favor bacterial adherence. In this case, the presence of more flexible pendant polymer chains favors molecular interactions and energy dissipation when the bacteria initially come in contact with the substrate.[36]

Given that adhesion involves two surfaces that interact through an interface, it is necessary to study the contributions of both systems. In this work, we have studied the role of elasticity and geometry in the phenomenon of bacterial adhesion to polymeric surfaces made of fibers. To this end, we first carried out experiments to determine differences in the population counts of three bacterial species, *P. aeruginosa* DSM 22644, *B. subtilis* DSM 10, and *S. aureus* DSM 20231, on polymeric substrates made of fibers of varying diameters. Polycaprolactone (PCL) was chosen to develop the fiber because of its extensive use in medical devices.[37] Second, we characterized the bacteria in terms of geometry (size and shape) and elasticity (Young's modulus). The resulting adhesive propensity was characterized in terms of an energy gain (ΔE) resulting from the balance between adhesion energy and deformation energy of the bacterial cell, which can be interpreted as an energy barrier necessary to remove the bacterial cell from the substrate. We identified two regimes; (1) where the radius of the fiber is larger than that of bacteria, $R_b \ll R_f$ and (2) where the radius of the fiber is similar to that of bacteria, $R_b \approx R_f$. The two regimes allow a consistent interpretation with the observed populations of bacteria on substrates with different fiber diameters.

https://dx.doi.org/10.1021/acsami.9b21060
ACS Appl. Mater. Interfaces 2020, 12, 14507−14517

MATERIALS AND METHODS

Materials. Polycaprolactone (Mw 80,000 g/mol) was purchased from Sigma-Aldrich. Dichloromethane (DCM), *N,N*-dimethylformamide (DMF), and chloroform were purchased from Merck. Deionized water with 0.055 μS/cm conductivity, 18.2 MΩcm resistivity, and a total organic carbon (TOC) content of less than 10 ppb was obtained from LabStar 4-DI.

Substrate Preparation. PCL fibers were electrospun with the basic Tong Li Tech electrospinning equipment. Prior to fiber processing, PCL polymer films were prepared by spin-coating on foil aluminum at 5000 rpm for 60 s from a 12% w/v PCL solution using chloroform as a solvent. To obtain polymeric substrates, the PCL-coated aluminum was then placed in the collector of the electrospinning equipment where the fibers were deposited. The fibers were prepared from 15% w/v PCL solutions using DCM/DMF mixtures as a solvent. The polymer solutions were electrospun with controlled voltages and flow rates to obtain fibers of varying diameters (see Table 1). A 20 gauge nozzle was used, with a distance of 20 cm between the needle and collector. The conductivity of polymer solutions was determined using a conductivity meter (Radiometer, CDM 83). The surface tension was determined using the ring method with a Du Nouy tensiometer. All measurements were performed at 25 °C.

Bacteria Incubation on the Substrates. Bacteria (*S. aureus* DSM 20231, *P. aeruginosa* DSM 22644, and *B. subtilis* DSM 10) were grown in a Luria Bertani culture broth at 37 °C for 16 h. The resulting cultures were then transferred to fresh media and standardized to 10^6 CFU/mL by measuring optical density at 600 nm. Parallel cultures were grown in an LB medium to ensure that the growth curves of the different bacteria are comparable. We obtained similar values of kinetic growth and generation time for *S. aureus* DSM 20231, *P. aeruginosa* DSM 22644, and *B. subtilis* DSM 10. A volume of 400 μL of this solution was deposited on 1-by-1 cm^2 polymeric substrates and incubated for 7 h. Samples were washed with 10 mL of a solution containing 0.01 M of sodium cacodylate/0.15 NaCl buffer at pH 7.4 and fixed with 1% glutaraldehyde for 2 h at room temperature. The samples were again rinsed in 0.01 M sodium cacodylate/0.15 M NaCl buffer at pH 7.0 and finally dehydrated in ascending grades of ethanol (30, 50, 70, 80, 90, and 100%). The dehydrated samples were then coated with thin films of Pt/Pd and observed by scanning electron microscopy operated at 5 kV. Five images were obtained from 10 different zones of each sample to select representative images.

Sample Preparation to Assess Adhesion Energy and the Young's Modulus. A positively charged microscope slide (Porlab) was cut into 1-by-1 cm^2 sections. A 0.2% poly(ethyleneimide) (750,000 Da; Aldrich) solution in MQ water was used to increase the charge on the glass surface.[38] The glasses were incubated with this solution for 5 h, rinsed with MQ water, and left to dry overnight. Ten milliliters of overnight culture in an LB medium of each bacterial species (*S. aureus* DSM 20231, *P. aeruginosa* DSM 22644, and *B. subtilis* DSM 10) was centrifuged, and collected cells were washed twice with 5 mL of 1 mM Tris, pH 7. The cell suspensions were prepared in 1 mL of the same buffer, and samples were extracted to check cell numbers and adjust the final concentration to 10^{11} cells/mL. A volume 100 μL of the cell suspension was put on the surface of the treated slides and incubated in darkness for 90 min. The glass slides were rinsed three times with Tris buffer to eliminate an excess of free/unadhered cells. The cell-covered slides were analyzed by AFM. To further assess adhesion energy, PCL substrates were prepared by spin-coating on 1-by-1 cm^2 microscope slides. A roughness (RMS of surface height) of R_q = 18 nm was evaluated by atomic force microscopy, while the typical lateral scale was approximately 200 nm.

Atomic Force Microscopy Images of Bacteria. Atomic force microscopy images were obtained from cells deposited on glass slides, using the Nanoscope IIIa in the tapping mode with a J scanner (Figure 1). Cells for AFM imaging were grown on surfaces previously treated with PEI and then washed with PBS at 37 °C for 24 h. Prior to AFM imaging in the air, bacteria that weakly adhered to the glass surface were rinsed with abundant milli-Q water and air dried in a clean environment at 30% relative humidity. Silicon nitride cantilevers (Olympus AC240TS) were used at a scan rate of 1 Hz, with a resonance frequency of 70−100 kHz, a curvature radius of 20 nm, and a stiffness of 5 N/m.

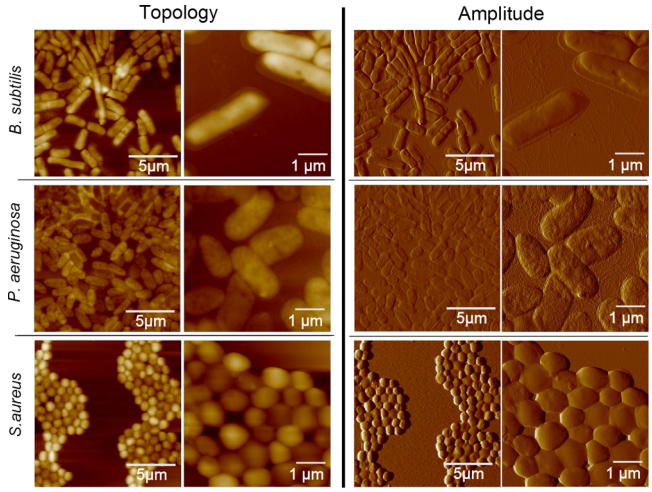

Figure 1. Typical AFM images of bacteria on glass surface.

Colloidal Probe to Assess Adhesion Energy and the Young's Modulus. Young's modulus of bacteria and bacteria−PCL surface adhesion energy were assessed by the colloidal probe technique using two distinct experimental configurations.[39,40] In the first configuration (1), bacteria were transferred to the colloidal sphere (see Figure 2a). Young's modulus of bacteria was determined from the features of the force extension curve obtained when bacteria was pushed against the PCL surface. Conversely, adhesion energy was obtained from the features of force curves in retraction. Silicon nitride cantilevers provided with a microsphere, 5 μm in diameter made of SiO_2 attached at one end (colloidal probe purchased from Novoscan PTGS), were immersed in drops of a 1% poly(ethyleneimmine) (PEI) solution for several minutes. After removing excess solution, the probes were dried and stored at 4 °C until use. To immobilize the bacteria (harvested as described above) on the colloidal probe, a pellet of the cells was manually transferred onto the PEI-coated microsphere by means of a micromanipulator (Narishige MHW-3), under a Nikon inverted microscope. A Nanoscope III AFM (Digital Instruments), picoForce module was used to measure the adhesion force between the colloidal sphere previously coated with the bacteria, and a thin film of PCL polymer deposited by spin coating onto a glass surface. In the second configuration (2), bacteria were grown on a glass surface (see Figure 2b), while a colloidal sphere of a 5 μm radius, made of PCL polymer (DiagPoly, PCL: polycaprolactone, from CD Creative Diagnostics), previously attached to a tipless cantilever, was pressed against the bacterial film. All colloidal probe experiments were conducted in 1 mM cell-filled TRIS buffer at a constant pH of 7.

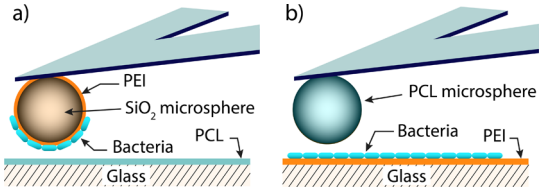

Figure 2. Colloidal probe configurations. (a) Bacteria on the colloidal sphere (glass) are gently pushed against the PCL surface (configuration 1). (b) The colloidal probe made of PCL sphere is pushed against a film of bacteria (configuration 2).

The two colloidal probe configurations were used to provide broad experimental conditions for mechanical assessment of bacteria.

https://dx.doi.org/10.1021/acsami.9b21060
ACS Appl. Mater. Interfaces 2020, 12, 14507−14517

Pushing a colloidal bacteria-coated glass sphere repeatedly against a solid surface progressively damages the bacterial layer. Instead, pushing a colloidal sphere made of desired polymeric material against a bacterial film located on a flat surface allows for making assessments by mechanical testing of distinct locations on the bacterial film in tandem with AFM imaging as a control for biofilm quality. It is remarkable that in our case the two configurations produced similar results.

The pulling and pushing forces were measured by AFM, with a scan rate of 0.3 Hz and a null scan size. The ramp size was approximately 300 nm, and the loading force was applied by setting the maximum deflection value (maximum force on bacteria of approximately 3−5 nN). Care was taken to minimize lateral and vertical compressing forces on the approach to avoid damaging the cell probe. Force curves were acquired automatically at distinct sample locations, and sufficient data for representative statistic were obtained. More than 150 force curves were acquired per sample, and each experiment was repeated at least three times with fresh bacteria for the three types of bacteria considered. Distinct areas of the sample were explored to obtain representative force curves with bacterial coverage. Analysis of the data includes regular statistics from which average values and their respective standard deviations were obtained and presented in tables in the following sections. The maximum pulling force was obtained from the cantilever deflection curves by multiplying the maximum cantilever deflection by cantilever stiffness. The thermal fluctuation method was employed to obtain cantilever stiffness.

Stiffness of bacteria: Young's modulus for bacteria was obtained as a fitting parameter through a suitable model expression for the approaching force curve. The compression response force of a thin elastic film of bacteria with a thickness of h and a Young's modulus of E, bound to a relatively hard substrate is[41]

$$F \approx \frac{16}{9} E R^{1/2} \delta^{3/2} [1 + 1.13\sqrt{R\delta}/h + 1.283 R\delta/h^2] \quad (1)$$

where R is the radius of curvature of the colloidal sphere, and δ is its penetration distance. Adhesion should be weak in the application of this model, as was the case here. Experimentally, the thickness "h" of the soft layer is the average value of the bacterial film (typically, the bacterial capsule thickness) at the scale of the size of the contact zone ($\sqrt{R\delta}$). The average Young's modulus for bacteria was obtained by fitting a representative number of force curves. A recent work by Xia el al.[42] dealt with possible viscoelastic effects on the mechanical response of films, as well as the effect of finite film thickness. Formulas provided by Xia et al.[42] may be more suitable than eq 1 in the presence of significant viscoelastic effects. In the case of our study, these effects are small (see discussion section) and are experimentally prevented by choosing a relatively slow loading speed of 0.3 μm/s.

Adhesion energy of bacteria: an approximate value of the work of adhesion was obtained by measuring adhesion force F_{adh}, which was determined directly by the magnitude of the snap-off force from the retraction curve. Because Young's modulus for bacteria revealed that the studied bacteria have outer layers of the soft material, we employed the Johnson−Kendall−Roberts formula,[43] which relates adhesion energy per unit area to adhesion force,

$$W_{adh} = \frac{2F_{adh}}{3\pi R} \quad (2)$$

RESULTS AND DISCUSSION

Fiber Characterization. PCL was dissolved in a solvent mixture dichloromethane/dimethylformamide (DCM/DMF) and electrospun to produce fibers with varying diameters. As shown in Table 1, the proportions of solvents used played an important role in the diameter of the final fiber. The solutions prepared with solvent mixtures with more DMF resulted in smaller fiber diameters due to the greater conductivity of the solutions and less surface tension. In general, DMF is mainly used to increase the conductivity of polymer solutions solution.[44] The SEM images in Figure 3 show the morphology

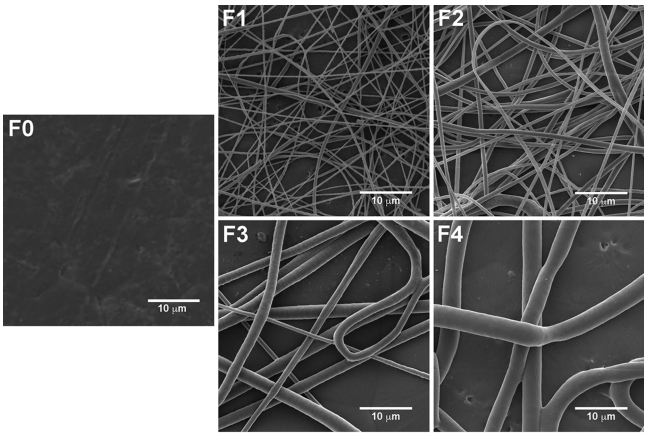

Figure 3. SEM images of flat PCL substrates without (F0) and with fibers of variable diameters (F1−F4).

of the substrates where F0 is a flat PCL surface prepared by spin-coating, while F1−F4 are flat surfaces covered with fibers of varying diameters. From left to right, the average fiber diameter increases by 0.4 ± 0.2 μm for F1, 0.8 ± 0.4 μm for F2, 1.8 ± 0.7 μm for F3, and 3.6 ± 0.3 μm for F4. These diameters are summarized in Table 1.

Bacterial Populations on Substrates with Fibers. Figure 4 shows bacteria adhering to the substrates after being washed with cacodylate buffer at pH 7. Blue bacteria correspond to *P. aeruginosa* DSM 22644, while pink and yellow are *B. subtilis* DSM 10S and *S. aureus* DSM 20231, respectively. The largest bacterial populations on all substrates were those of *P. aeruginosa* DSM 22644, while the smallest populations on all substrates were those of *S. aureus* DSM 20231. The populations of *P. aeruginosa* and *B. subtilis* were larger on substrates with F1 fibers (smaller fiber diameter) than on any other substrate, including flat substrates (F0).

It is possible to go beyond a global analysis (total populations) of the SEM images of adhering bacteria by identifying attachment sites representing distinguishable features of the substrate. Indeed, the sites where bacteria are in contact with the substrate can be located either on the plane (p) or on a fiber (f). However, it was possible to observe that one bacterial cell can be in contact with more than one site at the same time. Configurations in which bacteria are attached to one, two, or more fibers at the same time are labeled *1f*, *2f*, and so on. If bacterial cell is on the plane, it is in configuration *p*. Bacteria simultaneously attached to the plane and to one, two, or more fibers are in configuration *p1f*, *p2f*, and so on. We also use the notation *nf* to refer to an *n*-fiber attachment, and *pnf* to a plane-*n*-fiber attachment. Figure 5 shows possible configurations, together with a SEM image of *P. aeruginosa* in the corresponding configurations.

Having defined the possible adhesion configurations, we assessed the bacterial populations under particular configurations by counting contact sites for all the bacteria with the substrate. The subpopulations representing the configurations *p*, *1f*, *p1f*, *2f*, *p2f*, etc. were identified in all the SEM images. The first observation is that all bacteria are likely to adhere in configurations involving (1) a larger contact area or (2) a larger number of attachment sites. A second observation is that

https://dx.doi.org/10.1021/acsami.9b21060
ACS Appl. Mater. Interfaces 2020, 12, 14507−14517

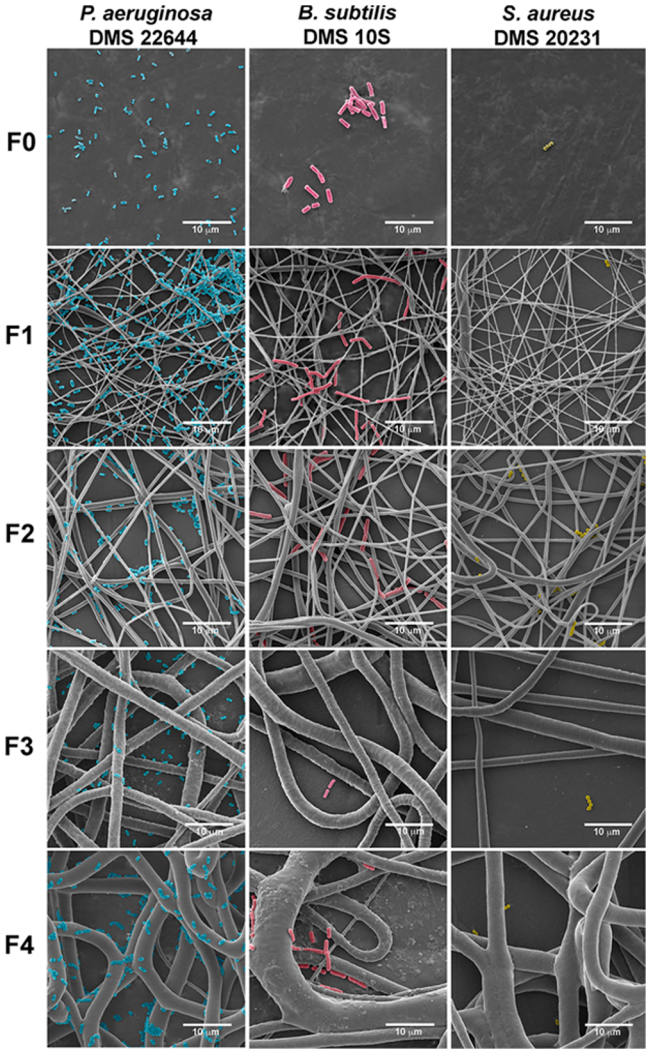

Figure 4. SEM images of *P. aeruginosa* DSM 22644, *B. subtilis* DSM 10S, and *S. aureus* DSM 20231 adhering to the substrates F0, F1, F2, F3, and F4.

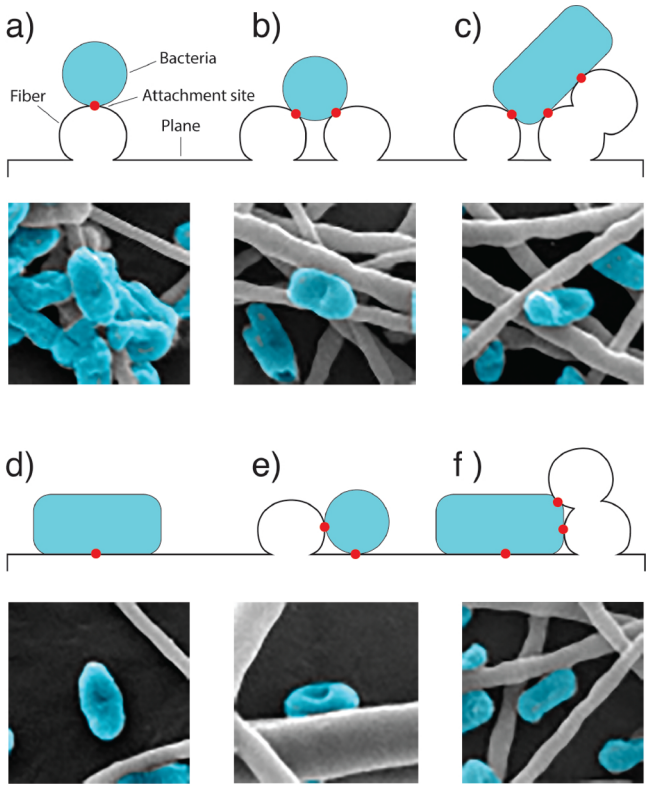

Figure 5. Different attachment configurations for *P. aeruginosa* DSM 22644: (a) one fiber (*1f*), (b) two fibers (*2f*), (c) three fibers (*3f*), (d) plane (*p*), (e) plane and one fiber (*p1f*), and (f) plane and two fibers (*p2f*).

even if a larger number of attachment sites increases adhesion, the populations in *nf* and *pnf* configurations decrease considerably with increasing *n*. This is because the probability that more and more fibers cross a region whose size is comparable to the largest dimension of the bacterial cell decreases with the number of fibers. The described mechanisms, one energy-related, and the other related to the geometry of the fiber network, imply different behaviors of the three studied bacteria, as observed in the SEM images.

Figure 6a–c plots the population fractions of the three bacteria with the observed configurations. Data have been obtained from a single representative image for each type of substrate (F1–F4), with the exception of *B. subtilis* on the F3 substrate (Figure 6b) where low populations are observed. Here, we used four images obtained from four independent preparations of the same type of substrate. The data for *P. aeruginosa* (Figure 6a) and *S. aureus* (Figure 6c) were obtained from the images shown in Figure 5. Data for Figure 6b were obtained from images shown in Figure S1 in the Supporting Information section. Figure 6a shows that *P. aeruginosa* has large *p1f* populations on all fiber substrates (F1–F4). However, with larger fiber diameters, *p2f* and *p3f* populations decrease and *1f* and *2f* populations increase. This behavior is because the number of *p1f* attachment sites is proportional to the α area fraction where this configuration is possible. A rough estimate gives $\alpha \sim Ll_b/A_0$ per unit of total area where L is total fiber length, A_0 is the total area, and l_b is the largest dimension of the bacterial cell. The area A covered by fibers scales as $A \sim LR_f$ where R_f is fiber diameter. The SEM images show that the ratio of fiber area to total area is roughly the same in all substrates, hence $A/A_0 \sim$ constant, implying that the total fiber length per unit area of substrate decreases as the inverse of fiber diameter ($L \sim A/R_f$). Consequently, $\alpha \sim l_b/R_f$, and the available sites for *p1f* attachment decrease with increasing fiber diameter. The same argument can be applied to the *p2f* configuration but taking into account a lower number of fiber crossings as L decreases (with increasing R_f). The increase in *1f* and *2f* configurations with larger fiber diameter is likely due to decreased fiber curvature, which become virtually flat if $R_f \gg R_b$ where R_b is the smallest dimension of the bacterial cell ($l_b = 2R_b$ if the bacteria are spherical). In contrast, larger order plane-fiber configurations like *p3f* and *p4f* become less populated with larger fiber diameters due to the low probability that two or more thick fibers cross in a region of size $\sim l_b$. The distributions on F1 and F2 substrates are notably very similar. This may be a statistical effect due to the large subpopulations of *P. aeruginosa* observed on two substrates with similarly thin fibers.

Figure 6b plots the population fractions of *B. subtilis*. Populations of these bacteria are one order of magnitude lower than that of *P. aeruginosa*. They differ from *P. aeruginosa* in that the largest *pnf* populations shift toward higher orders (*p3f* and *p4f*) with the thinnest fibers (F1 and F2). This behavior can be ascribed to the large longitudinal dimension, l_b, of *B. subtilis*,

https://dx.doi.org/10.1021/acsami.9b21060
ACS Appl. Mater. Interfaces 2020, 12, 14507–14517

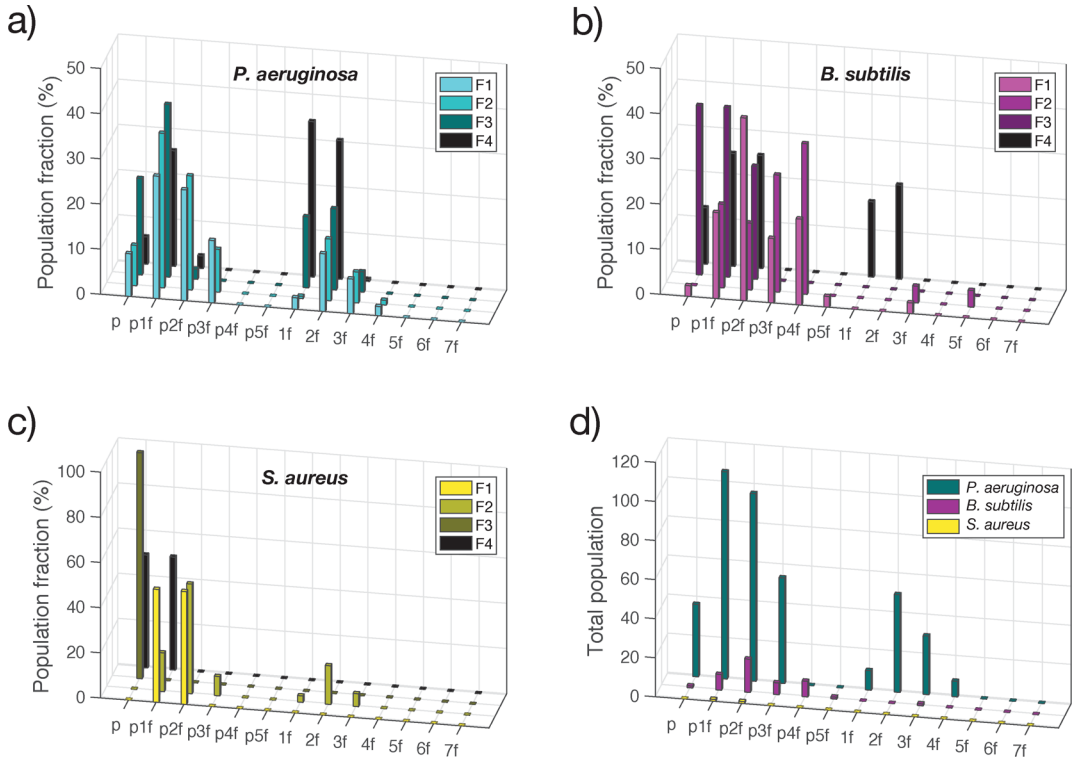

Figure 6. (a)−(c) Population fractions of bacteria with different observed attachment configurations: *P. aeruginosa* DSM 22644 (a), *B. subtilis* DMS 10S (b), and *S. aureus* DSM 20231 (c) on F1−F4 substrates, and (d) total populations of the three bacteria on the F1 substrate.

which allows these bacteria to attach to several fibers at the same time, if they cross over a region of size $\sim l_b$. Another efficient way to increase adhesion is to align with fibers. Some bacteria attached alongside a fiber in a *p1f* configuration can be seen in the F1, F2, and F4 substrates in Figure 4. Finally, Figure 6c represents the population fractions of *S. aureus*. The small populations of *S. aureus* rule out any rigorous statistical analysis. The populations are low on even the thinnest fibers, indicating that *S. aureus* attaches weakly to fibers and to planar surfaces (or thick fibers). We observe, however, that the distribution of subpopulations of *S. aureus* and *P. aeruginosa* in the F1 substrate is similar while differing from those of *B. subtilis*. Again, this might be due to the greater length of *B. subtilis*. Figure 6d plots the subpopulations of *P. aeruginosa*, *B. subtilis*, and *S. aureus* on the F1 substrate, comparing the three populations. Globally, *P. aeruginosa* attaches more to a substrate with a given fiber size than *B. subtilis*, which in turn attaches more than *S. aureus*.

These results clearly show that the fiber diameter affects the morphology of the mesh and therefore the distribution of sites (configurations) that facilitate bacterial adhesion. However, previous studies have considered only the effect of fiber diameter on bacterial adhesion. Abrigo et al.[13] claimed that meshes with fibers whose diameter is similar to the size of the bacteria increase bacterial adhesion, whereas Rumbo et al.[14] observed that a variable fiber diameter has no effect on bacterial adhesion. Our findings show that the random arrangement of fibers gives rise to distinguishable geometrical features where attachment is determined not only by the diameter of the fibers, but also by the quantity of binding sites.

Elasticity−Adhesion Interplay Model for Bacterial Adhesion to Fibers. Observed differences in bacterial subpopulations are due to shape (spherical or cylindrical), stiffness (Young's modulus), and adhesion energy. In this section, we present the typical values of these parameters for the bacteria considered in this work and a minimal model that incorporates their interplay. Force curves obtained with the two methodologies described in the previous section show a strongly nonlinear response of bacteria to compression (Figure 7). This concurs with the nonlinear law used to fit data in eq 1.

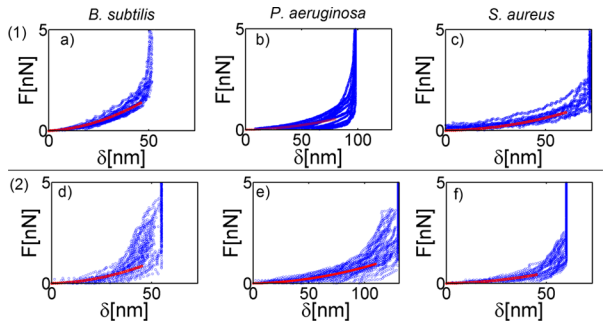

Figure 7. Typical compression curves of bacteria obtained through the experimental configurations presented in the Materials and Methods section. (1) Bacteria on a colloidal sphere pushed against a PCL surface. (2) Bacteria on a glass surface compressed by a PCL colloidal sphere.

However, the applied force strongly increases with deformation δ for values above 100 nm. This is due to the finite size of the bacterial capsule layer. Indeed, a much greater bacterial stiffness is observed with high levels of deformation where turgor pressure[45] on the cellular wall dominates the mechanical response. Table 2 shows the average Young's modulus obtained through this fitting procedure with a low level of deformation. The reported values are in the range of 5−40 kPa

https://dx.doi.org/10.1021/acsami.9b21060
ACS Appl. Mater. Interfaces 2020, 12, 14507−14517

Table 2. Summary of the Elastic and Adhesion Properties of Bacteria[a]

	Y. modulus (kPa)		F_{adh} (nN)		W_{adh} (mJ/m^2)				
bacterial cell	(1)	(2)	(1)	(2)	(1)	(2)	$\Delta E(\delta_{eq})$ (J)	diameter (μm)	length (μm)
B. subtilis	35 ± 22	34 ± 10	0.3 ± 0.2	0.4 ± 0.2	0.03 ± 0.02	0.06 ± 0.03	1.4×10^{-17}	0.8 ± 0.1	2.2 ± 0.6
P. aeruginosa	5 ± 3	6 ± 3	0.3 ± 0.2	0.4 ± 0.1	0.03 ± 0.02	0.05 ± 0.02	2.7×10^{-17}	0.8 ± 0.1	1.8 ± 0.3
S. aureus	12 ± 4	15 ± 8	0.9 ± 0.6	0.4 ± 0.1	0.08 ± 0.05	0.05 ± 0.02	4.6×10^{-19}	0.8 ± 0.2	0.8 ± 0.2

[a](1) Colloidal probe made SiO_2 microsphere covered with bacteria pushed against and retracted from a PCL film. (2) Colloidal probe made of PCL micro-sphere pushed against and retracted from bacteria film.

and are of the same order as those found independently for capsules of several bacteria: *K. pneumoniae* AJ218,[46] E_b = 12 ± 2 kPa; *S. putrefaciens* CN32,[47] E_b = 69 ± 15 kPa; *S. epidermidis* ATCC 35983,[48] E_b = 22 ± 4 kPa; *S. salivarius* HB-C12,[48] E_b = 13 ± 2 kPa; *S. aureus* NCTC 8325-4 Wild-type and NCTC 8325-4 pbp4,[48] E_b = 47 ± 26 kPa, and E_b = 10 ± 1 kPa, respectively.

It is important to note that the bacterial capsule may exhibit a viscoelastic response when the external stress is applied more rapidly than capsule can relax. To rule out any viscoelastic effect that may influence our Young's modulus measurements, we performed a loading−unloading cycle (force vs penetration) and evaluated the dissipated energy over one cycle as the area of the resulting hysteresis curve in the positive quadrant. The ratio of the dissipated energy to total energy, U_d/U_t, is a measure of the degree of viscous dissipation with respect to elastic energy and serves to establish a limit for the validity of our methodology. We found that for *P. aeruginosa*, *S. aureus*, and *B. subtilis*, U_d/U_t < 1%, < 10%, and < 7%, respectively, which leads to an overestimation of the Young's modulus of $\Delta E/E$ < 1%, < 5%, and < 4%, respectively. These values are lower than the corresponding dispersions resulting from the determination of the elastic moduli (Table 2). We conclude that capsule viscoelasticity does not significantly affect our measurements.

The retraction curves likewise illustrate the level of adhesion experienced by bacteria on the PCL surface (Figure 8). Indeed, the maximum retraction force, F_{adh}, W_{adh} through eq 2, Table 2 shows the average W_{adh} values obtained with the two techniques.

Spherical Bacteria: Interaction with the Substrate. In this section, we elucidate the role of bacterial elasticity (Young's modulus, E_b) and adhesion energy, W, on bacterial adherence to polymer surfaces. For simplicity, we consider the contact between a spherical and homogeneous bacterial cell

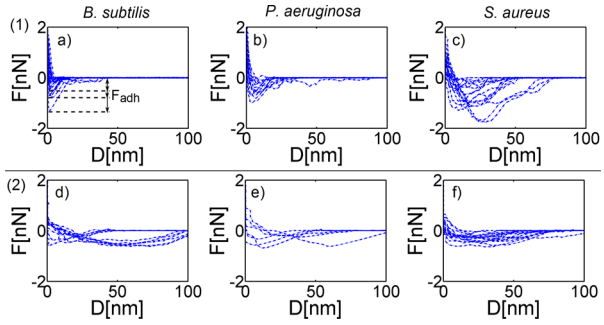

Figure 8. Typical pulling curves obtained through the experimental configurations presented in the Materials and Methods section. (1) Bacteria on colloidal sphere pulled from a PCL surface. (2) Bacteria on glass surface pulled by a colloidal sphere made of PCL. Adhesion force is identified as the maximum force in the retraction mode.

with a radius of R_b and a polymer fiber with a radius of R_f and a Young's modulus E_f. We note that a cylindrical bacterial cell interacting with a fiber is more realistic, but only differing by numeric factors of an order of one.[49] Regardless of the bacterial geometry, we assume that adhesion induces elastic penetration that is limited to a region smaller in size than the capsule thickness (the hard core dominated by turgor pressure is ignore[45]). We first demonstrate that despite the elastic energy cost due to bacterial deformation, there is a net energy gain when bacteria adhere to a fiber surface compared to with respect to the state in which bacteria do not adhere. This energy can be written as,

$$\Delta E = \frac{2}{5}\kappa\delta^{5/2} - \pi a^2 W, \tag{3}$$

where we have considered that elastic energy is characterized by the Hertz potential[43] for a penetration distance δ, with $\kappa = \frac{4}{3}E^* R^{*1/2}$, $\frac{1}{E^*} = \frac{1}{E_b} + \frac{1}{E_f}$, and $R^* = \frac{R_b R_f}{R_b + R_f}$. In addition, $a = \sqrt{R^*\delta}$ is the radius of the contact zone, and W is the adhesion energy. Minimizing ΔE as function of δ yields an optimum penetration distance, $\delta_{eq} = (\pi W R^*/\kappa)^{2/3}$, which allows for calculating the energy gain for the adhesion of bacteria to a surface, $\Delta E(\delta_{eq})$,

$$\Delta E(\delta_{eq}) \approx -\frac{\pi^{5/3}}{2}\frac{R^{*4/3}W^{5/3}}{E^{*2/3}} \tag{4}$$

Our measurements indicate that E_f (300 MPa) $\gg E_b$ (5−35 kPa, Table 2) and in experiments in flat surfaces, $R^* = R_b$, hence $\Delta E(\delta_{eq}) \approx -\frac{\pi^{5/3}}{2}\frac{R_b^{4/3}W^{5/3}}{E_b^{2/3}}$. In addition, measurements of bacterial adhesion force obtained by atomic force microscopy (AFM) provide typical values of F_{adh} = 1 nN for spherical bacteria (*S. aureus*), which leads to $W \approx 0.06$ mJ/m^2. The contact zone radius, $a = \sqrt{R_b\delta_{eq}}$, can be expressed as $a^3 \approx 3\pi W R_b^2/4E_b$, and is estimated at $a \approx 100$ nm. We note that the energy gain can be seen as an energy barrier to dislodging bacteria from the surface. Our measurements for *S. aureus* indicate that this energy is $\Delta E(\delta_{eq}) \approx 4.6 \times 10^{-19}$ J, which is two orders of magnitude greater than kT at ambient temperature (4×10^{-21} J). We also note that elastic deformation is confined to a small zone of the bacterial capsule. A capsule thickness of about 50 nm or even smaller is sufficient to provide adequate contact surface to sustain bacterial adhesion. However, when the size $\sim a$ of the bacterial deformation zone is larger than the capsule thickness, corrections may be required to consider the presence of the hard bacterial core.[41,50] Thus, both bulk elasticity and adhesion energy are important in bacterial adhesion. Strong adhesion together with low bulk elasticity result in an energy gain several orders of magnitude larger than thermal energy, indicating that bacteria

https://dx.doi.org/10.1021/acsami.9b21060
ACS Appl. Mater. Interfaces 2020, 12, 14507−14517

will strongly adhere to surfaces. The same considerations are valid for a bacterial cell attached to a thick fiber ($R_b \ll R_f$) in which case $R^* \approx R_b$. Based on the above, deformable bacteria can be expected to lodge in regions of the substrate that offer greater surface contact with minimum bulk changes. This is likely to occur at regions of fiber crossings.

We now discuss the case where the radius of the bacterial cell is similar to that of the fiber. Here, the cylindrical shape of the fiber must be taken into account. It can be shown that[43] $1/R^* = 1/R_b + 1/2R_f$, which for $R_b \approx R_f$ leads to $R^* \approx 2R_b/3$. According to eq 4, it is more favorable for bacteria to adhere to a flat surface than a curved filament. However, if the network of fibers is dense, bacteria can adhere using more than one contact. In the case of n contacts, the energy gain (eq 4) is simply multiplied by the number of contacts. Thus, bacteria can reach strong dislodging energy. Note that with $n = 2$, this energy is about 30% higher than that with a single contact on a flat surface.

Cylindrical Bacteria. This section considers the effect of the cylindrical shape of bacteria on adhesion, which is relevant for rod-like bacteria attached alongside fibers. As a rough estimate, we consider a bacterial cell with a perfectly cylindrical shape and neglect the effect of spherical caps. The energy gain due to the elastic deformation of a cylinder with radius R_1 and length l pushed against a surface with radius R_2 and a contact area of $2al$, where $a = \sqrt{R^*\delta}$ is written as:

$$\Delta E_c = \frac{\pi}{8} E^* l \delta^2 - 2lW\sqrt{R^*\delta}\, s \tag{5}$$

Minimizing eq 5 results in equilibrium deformation $\delta_{eq} = \left(\frac{4W}{\pi E^*}\right)^{2/3}$ and an energy barrier to dislodging cylindrical bacteria,

$$\Delta E_c(\delta_{eq}) \approx -\frac{3}{2}\left(\frac{4}{\pi}\right)^{1/4} \frac{W^{4/3} R^{*2/3} l}{E^{*1/3}} \tag{6}$$

To evaluate the importance of spherical ends with respect to the cylindrical part of a bacterial cell in the absorption energy, we compute the ratio of both contributions by maintaining the adhesion energy, the Young's modulus and the radius of the bacterial cell, constant,

$$\frac{\Delta E_s}{\Delta E_c} \approx 2\left(\frac{W}{E^* R^*}\right)^{1/3} \frac{R^*}{l} \tag{7}$$

As expected, the expression above indicates that for bacteria with large aspect ratio, $R_b/l \ll 1$, energy is dominated by the cylindrical contribution. Taking typical values, $W = 2 \times 10^{-5}$ J/m^2, $E^* = 3 \times 10^4$ Pa, and $R^* = 0.5 \times 10^{-6}$ m, we obtain, $2\left(\frac{W}{E^* R^*}\right)^{1/3} \approx 0.17$. We conclude that rounded ends of elongated bacteria with $R_b/l < 0.5$ contribute less than 15% of total energy. We therefore use the cylindrical approximation for the two elongated bacteria investigated in this work to estimate the energy necessary to remove a bacterial cell from the substrate (Table 2); *P. aeruginosa* and *B. subtilis* have higher $\Delta E_c(\delta_{eq})$ values than the spherical bacteria, *S. aureus*.

Elasticity–Adhesion Model and Bacteria Populations. The observed populations of the three bacteria on substrates with fibers of given diameters can be interpreted in the light of the elasticity–adhesion model. According to (4) and the discussion that follows this equation, bacterial adhesion to a substrate can be enhanced by the following mechanisms: by (*i*) increasing the adhesion energy, W, (*ii*) decreasing Young's modulus, E_b, of the bacteria, (*iii*) increasing the local radius of curvature of the substrate, (*iv*) increasing the number of attachment sites, n, or (*v*) aligning with a fiber (only relevant for rod-like bacteria, see eq 6). Of the five mechanisms, *i*–*ii* are of physical nature, while *iii*–*v* have geometrical origins. As regards *iii*, we note that $R^* = R_b/(1 + R_b/R_f)$, hence R^* increases with R_f. In the discussion that follows, we assume that W is constant.

According to the model, soft bacteria like *P. aeruginosa* preferentially attach to surfaces with low or vanishing curvature (mechanism *ii*). This behavior is indeed observed, and supported by Figure 6a in which the *1f* population fractions systematically grow with increasing fiber diameter, while the *p* population fractions remain almost constant (average ∼12%). The *1f* subpopulations of *P. aeruginosa* were very low with the thinnest fibers in contrast to the larger subpopulations with higher order configurations like *2f*, *p1f*, and *p2f*. This can be attributed to the increase in energy as the number of contact points increases (mechanism *iv*). Direct observations also show that rod-like shaped bacteria like *P. aeruginosa* and *B. subtilis* frequently attach alongside fibers in *p1f* configuration. This is consistent with the increase in energy associated with parallel cylinder–cylinder contact (mechanism *v*).

Although *B. subtilis* and *P. aeruginosa* are similar in shape, they differ in stiffness (see Table 2). Our model predicts that *B. subtilis* is less adherent than *P. aeruginosa* according to mechanism *ii*. Observed populations of *B. subtilis* were in fact smaller than those of *P. aeruginosa* on all substrates. However, the greater length of *B. subtilis* allows these bacteria to attach in higher order configurations like *p4f* and *3f*, which are not observed for *P. aeruginosa*, as shown in Figure 6a,b. If we consider the *nf* and *pnf* subpopulations of *P. aeruginosa*, we observe a decrease with increasing orders of *n*. This may be a geometrical effect. Although these configurations are progressively more favorable in terms of energy, the probability that a certain number of fibers cross in a small region the size of the bacterial cell decreases with the number of fibers.

The low population of *B. subtilis* in the F3 substrate is striking. According to the model, this is the result of two antagonistic effects whose preponderance operates in opposite ways when the fiber size is modified. Indeed, adhesive propensity is enhanced by increasing the radius of the fibers (mechanism *iii*) or by increasing the number of contacts (mechanism *iv*). The first mechanism is characteristic of thick fibers (F4), while the second is characteristic of thin ones (F1 and F2). To rule out any abnormal data, we counted the populations of *B. subtilis* on five regions of the F3 sample. The corresponding SEM image in Figure 4 is representative of the general low level of adhesion of *B. subtilis* to the F3 substrate.

All mechanisms play against adhesion for stiff and almost spherical bacteria like *S. aureus*. The possibility to attach to more than one fiber at the same time is decreased by its oval, nearly spherical shape, and the alignment with fibers is not applicable (mechanism *v*). Populations of *S. aureus* were very low with all fiber sizes in our experiments, which can be noted in Figure 4 where a few bacteria are attached simultaneously to the plane and a fiber (*p1f*), or to two (*2f*), or three (*3f*) fibers (see also Figure 6c). This indicates that mechanism *iv* is the most efficient way to attach to fibers.

Kargar et al.[51] demonstrated the importance of the effect of substrate topographic curvature on bacterial adhesion. These authors studied ordered substrates consisting of surfaces

https://dx.doi.org/10.1021/acsami.9b21060
ACS Appl. Mater. Interfaces 2020, 12, 14507−14517

covered with straight and parallel fibers with controlled spacing between them. Even though Kargar et al. used regular substrates that differed significantly from those used in our study, their conclusions were the same: a greater bacterial deformation implies less adherence because of a higher adhesion energy cost. Our work provides a new perspective by considering the elastic energy required to deform bacteria accommodating to the topography of the surface to which it adheres and by establishing a criterion based on an energy balance that determines the adhesive propensity. In addition to adhesion energy, this balance depends on Young's modulus for bacteria, bacterial shape and dimensions, and fiber radius, all parameters that have been measured experimentally.

Bacterial adhesion is a complex phenomenon where the different attractive and repulsive interactions at the bacterium−substrate interface determine the propensity for a bacterial cell to attach. Although the interactions depend on the chemical nature of the substrate (wettability, surface energy, chemical composition, and charge), on the characteristics of the bacterial surface (hydrophobicity, chemical composition of the membrane/cell wall, charge, surface structures), together with environmental factors like pH, ionic strength, and temperature, the application of our model can be extended to the study of the adhesion of bacteria on fibers with a different chemical composition and to other strands of bacteria. Any change in these interactions will change the value of the total adhesion energy and consequently the energy gain, ΔE, which we interpret as the energy required to detach a bacterial cell from the substrate. The same model considers the topographic characteristics of the surface, which allows a more comprehensive evaluation of the overall tendency of bacteria to adhere to surfaces.

CONCLUSIONS

We studied the adhesion of three kinds of bacteria to heterogeneous surfaces considering for the first time the effect of the elasticity (stiffness) of the bacteria. Using substrates covered with electrospun fibers of varying sizes, we counted populations of bacteria lodged on distinguishable substrate features (single fibers, edges formed by a fiber and the plane, fiber crossings, etc.). From a balance between surface adhesion energy and the energy to elastically deform bacteria to increase its contact area, we defined the energy gain, ΔE, which could be significant in assessing the adhesive propensity of bacteria. Large gains, hence strong adhesion, arise from low levels of bacterial stiffness and low surface curvature (e.g., thick fibers), whereas weak adhesion is expected with high levels of stiffness and high curvature (e.g., thin fibers). This analysis considers only the physical aspects of the adhesion process. If we add the possibility of attachment to several sites simultaneously, adhesive propensity can be increased by increasing the number of contacts or alignments with fibers in the case of rod-like bacteria. This adds a geometric mechanism to the overall adhesion process that depends on the topography of the substrate. Our model predicts that bacterial adhesion is weak with very small nanometric fibers ($R_f \ll R_b$), as the relevant radius of curvature in this case is that of the fiber. However, adhesion could be enhanced with a higher density of fibers that increases the number of contact points. The low populations of *P. aeruginosa* and *B. subtilis* at an intermediate fiber size (F3) suggest the existence of an optimal fiber size such that the overall adhesion of bacteria is minimized. Indeed, thick fibers allow increased adherence in contrast to thin ones due to the increase in energy gain ΔE with greater local radius of curvature of the substrate. While thin fiber substrates allow increased energy gain through multiple site attachment, the same does not apply for substrates with thick fibers where the available sites for such configurations are less likely to exist. Our findings can then be useful in the design of antibiotic-free antimicrobial devices.

New knowledge on how bacterial elasticity and shape determine bacterial adhesion to heterogeneous surfaces can provide guidelines in developing novel surfaces to enhance control over initial adhesion and populations of adhering bacteria, particularly with surfaces made of fibers, which have scarcely been explored to date. We note however that future works should take into account specific structural and compositional characteristics of bacteria, and how these influence adhesion.

L.T., F.M., N.G., and M.U. received funding from Conicyt-Chile through Fondecyt projects 11160230 (L.T.), 1161010 (F.M.), 1160702 (N.G.), 1191467 (M.U.), and 1200853 (L.T.). E.H. was funded by DICYT 041931HH, Vicerrectoría de Investigación, Desarrollo e Innovación, Universidad de Santiago de Chile. Funding was also provided by Fondequip project EQM 130149 and PAI-Conicyt project 79170015.

ASSOCIATED CONTENT

Supporting Information

The Supporting Information is available free of charge at https://pubs.acs.org/doi/10.1021/acsami.9b21060.

SEM images of *B. subtilis* used for Figure 6b in the main article (PDF)

AUTHOR INFORMATION

Corresponding Authors

Laura Tamayo − *Departamento de Química, Facultad de Ciencias, Universidad de Chile, Santiago 3425, Chile;* orcid.org/0000-0003-1159-5305; Email: laura.tamayo@uchile.cl

Francisco Melo − *Departamento Física, Facultad de Ciencia, Universidad de Santiago de Chile, Santiago 3493, Chile; Center for Soft Matter Research, SMAT-C, Santiago 3363, Chile;* Email: francisco.melo@usach.cl

Authors

Leonardo Caballero − *Departamento Física, Facultad de Ciencia, Universidad de Santiago de Chile, Santiago 3493, Chile; Center for Soft Matter Research, SMAT-C, Santiago 3363, Chile*

Eugenio Hamm − *Departamento Física, Facultad de Ciencia, Universidad de Santiago de Chile, Santiago 3493, Chile*

M. Díaz − *Laboratorio de Comunicación Bacteriana, Departamento de Biología, Facultad de Ciencias, Universidad de Chile, Santiago 3425, Chile*

M. S. Leal − *Departamento de Química, Facultad de Ciencias, Universidad de Chile, Santiago 3425, Chile*

N. Guiliani − *Laboratorio de Comunicación Bacteriana, Departamento de Biología, Facultad de Ciencias, Universidad de Chile, Santiago 3425, Chile*

M. D. Urzúa − *Departamento de Química, Facultad de Ciencias, Universidad de Chile, Santiago 3425, Chile;* orcid.org/0000-0002-1894-2384

Complete contact information is available at: https://pubs.acs.org/10.1021/acsami.9b21060

https://dx.doi.org/10.1021/acsami.9b21060
ACS Appl. Mater. Interfaces 2020, 12, 14507−14517

Notes

The authors declare no competing financial interest.

REFERENCES

(1) Sanders, J. E. Medical Devices Comprising Small Fiber Biomaterials, and Methods of Use, U.S. Patent No. 7,947,069. *Washington, DC: U.S. Patent and Trademark Office*. 2011.

(2) Arinzeh, T. L.; Weber, N.; Jaffe, M. Electrospun Electroactive Polymers for Regenerative Medicine Applications, U.S. Patent Application No. 10,052,412. 2018.

(3) Troxel, K. S.; Stone, K. T. Suture Anchor with Soft Anchor of Electrospun Fibers, U.S. Patent No. 9,974,534. *Washington, DC: U.S. Patent and Trademark Office*. 2018.

(4) Jafari, H.; Shahrousvand, M.; Kaffashi, B. Reinforced Poly(ϵ-caprolactone) Bimodal Foams via Phospho-Calcified Cellulose Nanowhisker for Osteogenic Differentiation of Human Mesenchymal Stem Cells. *ACS Biomater. Sci. Eng.* **2018**, *4*, 2484−2493.

(5) Qing, H.; Jin, G.; Zhao, G.; Huang, G.; Ma, Y.; Zhang, X.; Sha, B.; Luo, Z.; Lu, T. J.; Xu, F. Heterostructured Silk-nanofiber-reduced Graphene Oxide Composite Scaffold for SH-SY5Y Cell Alignment and Differentiation. *ACS Appl. Mater. Interfaces* **2018**, *10*, 39228−39237.

(6) Ribba, L.; Tamayo, L.; Flores, M.; Riveros, A.; Kogan, M. J.; Cerda, E.; Goyanes, S. Asymmetric Biphasic Hydrophobic/Hydrophilic Poly(lactic acid)−polyvinyl Alcohol Meshes with Moisture Control and Noncytotoxic Effects for Wound Dressing Applications. *J. Appl. Polym. Sci.* **2019**, *136*, 47369.

(7) Tamayo-Ramos, J. A.; Rumbo, C.; Caso, F.; Rinaldi, A.; Garroni, S.; Notargiacomo, A.; Romero-Santacreu, L.; Cuesta-López, S. Analysis of Polycaprolactone Microfibers as Biofilm Carriers for Biotechnologically Relevant Bacteria. *ACS Appl. Mater. Interfaces* **2018**, *10*, 32773−32781.

(8) Zheng, Y.; He, L.; Asiamah, T. K.; Otto, M. Colonization of Medical Devices by Staphylococci. *Environ. Microbiol.* **2018**, *20*, 3141−3153.

(9) Reid, G. Biofilms in Infectious Disease and on Medical Devices. *Int. J. Antimicrob. Agents* **1999**, *11*, 223−226.

(10) Pierce, G. E. Pseudomonas aeruginosa, Candida albicans, and Device-related Nosocomial Infections: Implications, Trends, and Potential Approaches for Control. *J. Ind. Microbiol. Biotechnol.* **2005**, *32*, 309−318.

(11) Chastre, J.; Fagon, J.-Y. Ventilator-associated Pneumonia. *Am. J. Respir. Crit. Care Med.* **2002**, *165*, 867−903.

(12) Yetkin, G.; Otlu, B.; Cicek, A.; Kuzucu, C.; Durmaz, R. Clinical, Microbiologic, and Epidemiologic Characteristics of Pseudomonas aeruginosa Infections in a University Hospital, Malatya, Turkey. *Am. J. Infect. Control* **2006**, *34*, 188−192.

(13) Abrigo, M.; Kingshott, P.; McArthur, S. L. Electrospun Polystyrene Fiber Diameter Influencing Bacterial Attachment, Proliferation, and Growth. *ACS Appl. Mater. Interfaces* **2015**, *7*, 7644−7652. PMID: 25798788.

(14) Rumbo, C.; Tamayo-Ramos, J. A.; Caso, M. F.; Rinaldi, A.; Romero-Santacreu, L.; Quesada, R.; Cuesta-López, S. Colonization of Electrospun Polycaprolactone Fibers by Relevant Pathogenic Bacterial Strains. *ACS Appl. Mater. Interfaces* **2018**, *10*, 11467−11473.

(15) Hermansson, M. The DLVO Theory in Microbial Adhesion. *Colloids Surf., B* **1999**, *14*, 105−119.

(16) Katsikogianni, M.; Missirlis, Y. Concise Review of Mechanisms of Bacterial Adhesion to Biomaterials and of Techniques used in Estimating Bacteria-material Interactions. *Eur. Cell. Mater.* **2004**, *8*, 37−57.

(17) Ammar, Y.; Swailes, D.; Bridgens, B.; Chen, J. Influence of Surface Roughness on the Initial Formation of Biofilm. *Surf. Coat. Technol.* **2015**, *284*, 410−416.

(18) Cheng, Y.; Feng, G.; Moraru, C. I. Micro- and Nanotopography Sensitive Bacterial Attachment Mechanisms: A Review. *Front. Microbiol.* **2019**, *10*, DOI: 10.3389/fmicb.2019.00191.

(19) Dhaliwal, J. S.; Rahman, N. A.; Knights, J.; Ghani, H.; de Albuquerque Junior, R. F. The Effect of Different Surface Topographies of Titanium Implants on Bacterial Biofilm: A Systematic Review. *SN Appl. Sci.* **2019**, *1*, 615.

(20) de León, A. S.; Rodríguez-Hernández, J.; Cortajarena, A. L. Honeycomb Patterned Surfaces Functionalized with Polypeptide Sequences for Recognition and Selective Bacterial Adhesion. *Biomaterials* **2013**, *34*, 1453−1460.

(21) Doll, P. W.; Al-Ahmad, A.; Bacher, A.; Muslija, A.; Thelen, R.; Hahn, L.; Ahrens, R.; Spindler, B.; Guber, A. E. Fabrication of Silicon Nanopillar Arrays by Electron Beam Lithography and Reactive Ion Etching for Advanced Bacterial Adhesion Studies. *Mater. Res. Express* **2019**, *6*, No. 065402.

(22) Arango-Santander, S.; Pelaez-Vargas, A.; Freitas, S. C.; García, C. A Novel Approach to Create an Antibacterial Surface Using Titanium Dioxide and a Combination of Dip-pen Nanolithography and Soft Lithography. *Sci. Rep.* **2018**, *8*, 15818.

(23) Renner, L. D.; Weibel, D. B. Physicochemical Regulation of Biofilm Formation. *MRS Bull.* **2011**, *36*, 347−355.

(24) Mitik-Dineva, N.; Wang, J.; Mocanasu, R. C.; Stoddart, P. R.; Crawford, R. J.; Ivanova, E. P. Impact of nano-topography on bacterial attachment. *Biotechnol. J.* **2008**, *3*, 536−544.

(25) Helbig, R.; Günther, D.; Friedrichs, J.; Rößler, F.; Lasagni, A.; Werner, C. The Impact of Structure Dimensions on Initial Bacterial Adhesion. *Biomater. Sci.* **2016**, *4*, 1074−1078.

(26) Hizal, F.; Rungraeng, N.; Lee, J.; Jun, S.; Busscher, H. J.; van der Mei, H. C.; Choi, C.-H. Nanoengineered Superhydrophobic Surfaces of Aluminum with Extremely Low Bacterial Adhesivity. *ACS Appl. Mater. Interfaces* **2017**, *9*, 12118−12129. PMID: 28291321

(27) Bagherifard, S.; Hickey, D. J.; de Luca, A. C.; Malheiro, V. N.; Markaki, A. E.; Guagliano, M.; Webster, T. J. The Influence of Nanostructured Features on Bacterial Adhesion and Bone cell Functions on Severely Shot Peened 316L Stainless Steel. *Biomaterials* **2015**, *73*, 185−197.

(28) Ivanova, E. P.; Truong, V. K.; Webb, H. K.; Baulin, V. A.; Wang, J. Y.; Mohammodi, N.; Wang, F.; Fluke, C.; Crawford, R. J. Differential Attraction and Repulsion of Staphylococcus aureus and Pseudomonas aeruginosa on Molecularly Smooth Titanium Films. *Sci. Rep.* **2011**, *1*, 165.

(29) Miguel, S. P.; Figueira, D. R.; Simões, D.; Ribeiro, M. P.; Coutinho, P.; Ferreira, P.; Correia, I. J. Electrospun Polymeric Nanofibres as Wound Dressings: A Review. *Colloids Surf., B* **2018**, *169*, 60−71.

(30) Li, X.; Wang, X.; Yao, D.; Jiang, J.; Guo, X.; Gao, Y.; Li, Q.; Shen, C. Effects of Aligned and Random Fibers with Different Diameter on Cell Behaviors. *Colloids Surf., B* **2018**, *171*, 461−467.

(31) De Cesare, F.; Di Mattia, E.; Zussman, E.; Macagnano, A. A Study on the Dependence of Bacteria Adhesion on the Polymer Nanofibre Diameter. *Environ. Sci.: Nano* **2019**, *6*, 778−797.

(32) Zhang, J.; Huang, J.; Say, C.; Dorit, R. L.; Queeney, K. T. Deconvoluting the Effects of Surface Chemistry and Nanoscale Topography: Pseudomonas aeruginosa Biofilm Nucleation on Si-based Substrates. *J. Colloid Interface Sci.* **2018**, *519*, 203−213.

(33) An, Y. H.; Friedman, R. J.; Draughn, R. A.; Smith, E. A.; Nicholson, J. H.; John, J. F. Rapid Quantification of Staphylococci Adhered to Titanium Surfaces Using Image Analyzed Epifluorescence Microscopy. *J. Microbiol. Methods* **1995**, *24*, 29−40.

(34) Medilanski, E.; Kaufmann, K.; Wick, L. Y.; Wanner, O.; Harms, H. Influence of the Surface Topography of Stainless Steel on Bacterial Adhesion. *Biofouling* **2002**, *18*, 193−203.

(35) Lichter, J. A.; Thompson, M. T.; Delgadillo, M.; Nishikawa, T.; Rubner, M. F.; Van Vliet, K. J. Substrata Mechanical Stiffness Can Regulate Adhesion of Viable Bacteria. *Biomacromolecules* **2008**, *9*, 1571−1578. PMID: 18452330

(36) Straub, H.; Bigger, C. M.; Valentin, J.; Abt, D.; Qin, X.-H.; Eberl, L.; Maniura-Weber, K.; Ren, Q. Bacterial Adhesion on Soft Materials: Passive Physicochemical Interactions or Active Bacterial Mechanosensing? *Adv. Healthcare Mater.* **2019**, *8*, 1801323.

(37) Nyitray, C. E.; Chang, R.; Faleo, G.; Lance, K. D.; Bernards, D. A.; Tang, Q.; Desai, T. A. Polycaprolactone Thin-film Micro- and

Nanoporous Cell-encapsulation Devices. *ACS Nano* **2015**, *9*, 5675−5682.
(38) Velegol, S. B.; Logan, B. E. Contributions of Bacterial Surface Polymers, Electrostatics, and Cell Elasticity to the Shape of AFM Force Curves. *Langmuir* **2002**, *18*, 5256−5262.
(39) Butt, H.-J.; Cappella, B.; Kappl, M. Force Measurements with the Atomic Force Microscope: Technique, Interpretation and Applications. *Surf. Sci. Rep.* **2005**, *59*, 1−152.
(40) Caballero, L.; Mena, J.; Morales-Alvarez, A.; Kogan, M. J.; Melo, F. Assessment of the Nature Interactions of β-Amyloid Protein by a Nanoprobe Method. *Langmuir* **2015**, *31*, 299−306. PMID: 25486322
(41) Dimitriadis, E. K.; Horkay, F.; Maresca, J.; Kachar, B.; Chadwick, R. S. Determination of Elastic Moduli of Thin Layers of Soft Material Using the Atomic Force Microscope. *Biophys. J.* **2002**, *82*, 2798−2810.
(42) Xia, Y.; Duan, P.; Chen, J. Modelling the Nanomechanical Responses of Biofilms Grown on the Indenter Probe. *Processes* **2018**, *6*, 84.
(43) Johnson, K. L., Ed. *Contact Mechanics*; Cambridge University Press: New York, 1987.
(44) Uyar, T.; Besenbacher, F. Electrospinning of Uniform Polystyrene Fibers: The Effect of Solvent Conductivity. *Polymer* **2008**, *49*, 5336−5343.
(45) Mularski, A.; Wilksch, J. J.; Hanssen, E.; Strugnell, R. A.; Separovic, F. Atomic Force Microscopy of Bacteria Reveals the Mechanobiology of Pore Forming Peptide Action. *Biochim. Biophys. Acta* **2016**, *1858*, 1091−1098.
(46) Mularski, A.; Wilksch, J. J.; Wang, H.; Hossain, M. A.; Wade, J. D.; Separovic, F.; Strugnell, R. A.; Gee, M. L. Atomic Force Microscopy Reveals the Mechanobiology of Lytic Peptide Action on Bacteria. *Langmuir* **2015**, *31*, 6164−6171. PMID: 25978768
(47) Gaboriaud, F.; Parcha, B. S.; Gee, M. L.; Holden, J. A.; Strugnell, R. A. Spatially Resolved Force Spectroscopy of Bacterial Surfaces Using Force-volume Imaging. *Colloids Surf., B* **2008**, *62*, 206−213.
(48) Chen, Y.; Norde, W.; van der Mei, H. C.; Busscher, H. J. Bacterial Cell Surface Deformation under External Loading. *mBio* **2012**, *3*, No. e00378.
(49) Puttock, M. J.; Thwaite, E. G. *Elastic Compression of Spheres and Cylinders at Point and Line Contact*; National Standards Laboratory Technical Paper: *25*, 1969.
(50) Wolf, S. L. P.; Caballero, L.; Melo, F.; Cölfen, H. Gel-Like Calcium Carbonate Precursors Observed by in situ AFM. *Langmuir* **2017**, *33*, 158−163. PMID: 27992206
(51) Kargar, M.; Wang, J.; Nain, A. S.; Behkam, B. Controlling Bacterial Adhesion to Surfaces Using Topographical Cues: A Study of the Interaction of Pseudomonas aeruginosa with Nanofiber-textured Surfaces. *Soft Matter* **2012**, *8*, 10254−10259.

https://dx.doi.org/10.1021/acsami.9b21060
ACS Appl. Mater. Interfaces 2020, 12, 14507−14517